Proton-responsive ligands promote atmospheric CO_2 capture and accelerate catalytic CO_2/HCO_2^- interconversion

Jeffrey M. Barlow[1], Nikita Gupta[1,2], Ksenija D. Glusac[1,2], David M. Tiede[1], and David M. Kaphan[1*]

[1]Chemical Sciences and Engineering Division, Argonne National Laboratory, Lemont, Illinois 60439, United States.

[2]Department of Chemistry, University of Illinois Chicago, Chicago, Illinois 60607, United States.

KEYWORDS: Reactive CO_2 capture, CO_2 capture, direct air capture, DAC, CO_2 reduction, hydride transfer, catalysis, electrochemistry, electrocatalysis.

ABSTRACT: The synthesis and investigation of $[Rh(DHMPE)_2][BF_4]$ (**1**) is reported. **1** features proton-responsive 1,2-bis(di(hydroxymethyl)phosphino)ethane (DHMPE) ligands, which readily capture CO_2 from atmospheric sources upon deprotonation. The protonation state of the DHMPE ligand was observed to have a significant impact on the catalytic reactivity of **1** with CO_2. Deprotonation and CO_2 binding to **1** results in a ~10-fold rate enhancement in catalytic degenerate CO_2 reduction with formate, monitored by $^{12}C/^{13}C$ isotope exchange between $H^{12}CO_2^-$ and $^{13}CO_2$. Studies performed using a similar complex lacking hydroxyl ligand functionality ($[Rh(DEPE)_2][BF_4]$ where DEPE = 1,2-bis(diethylphosphino)ethane) do not show the same rate enhancements when base is added. CO_2 binding to **1** is proposed to facilitate pre-organization of formate/ CO_2 in the transition state to lower the activation energy and increase the observed catalytic rate. Incorporation of proton-responsive DHMPE ligands not only permits CO_2 capture from air, but also provides a unique approach to accelerate the kinetics of catalytic CO_2 reduction to formate.

A core challenge in achieving carbon-neutral energy and manufacturing technologies lies in the development of processes that link direct capture of atmospheric CO_2 to efficient catalytic conversion.[1–3] While significant progress has been made in both CO_2 capture and conversion fields separately, few examples of efficient combined CO_2 capture and conversion (CCC) systems exist. Several classes of nucleophiles have been utilized for reversible CO_2 capture from atmospheric concentrations including: alcohols/alkoxides, amines, and metal oxides/hydroxides.[4–7] These systems typically require heat or addition of acid to trigger CO_2 release however, resulting in stunted efficiencies and can be incompatible with many CO_2 reduction catalysts. "Reactive CO_2 capture" aims to minimize the energetic losses intrinsic to many CCC approaches (primarily arising from CO_2 release and concentration steps) by directly reducing captured CO_2 species, thereby combining both the CO_2 capture and conversion steps into a single process.[8] While reactive capture provides a promising approach to CCC, the field is in its nascent stages, with few examples, and those reported remain inefficient, either lacking selectivity or relying upon hydrogenation at high temperatures and pressures of H_2.[8–11]

The reduction of CO_2 into formate historically suffers from sluggish kinetics, which has been attributed to the high self-exchange reorganization energies involved for hydride transfer to CO_2.[12] Hazari and coworkers have shown that hydride transfer can be significantly accelerated by the introduction of exogenous Lewis acids, however the approach only works for metal hydride species following a specific "outer-sphere" pathway in certain solvents.[13–15] More recently, the Berben group has utilized pre-equilibrium hydride formation with their iron cluster catalyst systems to increase the kinetics of hydride transfer while simultaneously lowering overpotential.[16] While promising, these approaches have limited applicability. Currently, there are no reported methods that can be used for non-cluster complexes that proceed via "inner-sphere" or concerted hydride transfer pathways.[15]

Herein we report the synthesis and investigation of $[Rh(DHMPE)_2][BF_4]$ (**1,** Scheme 1), a coordination complex that combines an electron-rich Rh(I) metal center with a ligand framework containing CO_2-capture functionality. Upon deprotonation of a hydroxyl group on the DHMPE ligand, the resulting alkoxide is found to readily bind CO_2 at atmospheric concentrations to form an alkyl carbonate species. Furthermore, the CO_2 bound species is observed to catalyze CO_2/HCO_2^- interconversion with significantly accelerated rates, displaying roughly an order of magnitude rate increase of catalytic $^{12}C/^{13}C$ isotope exchange (between $H^{12}CO_2^-$ and $^{13}CO_2$) compared to solutions of **1** in the absence of base, where CO_2 binding to DHMPE does not occur. The incorporation of CO_2 binding functionality into the ligand framework of **1** is hypothesized to pre-organize formate/CO_2 through secondary coordination sphere interactions, resulting in acceleration of CO_2/HCO_2^- interconversion when CO_2 is bound, which provides valuable insight for the design of efficient reactive CO_2 capture systems that combine direct air capture (DAC) with catalytic conversion into value-added products.

Scheme 1. Proposed Deprotonation and CO_2 Binding of $[Rh(DHMPE)_2][BF_4]$ (1) and Structure of $[Rh(DEPE)_2][BF_4]$.

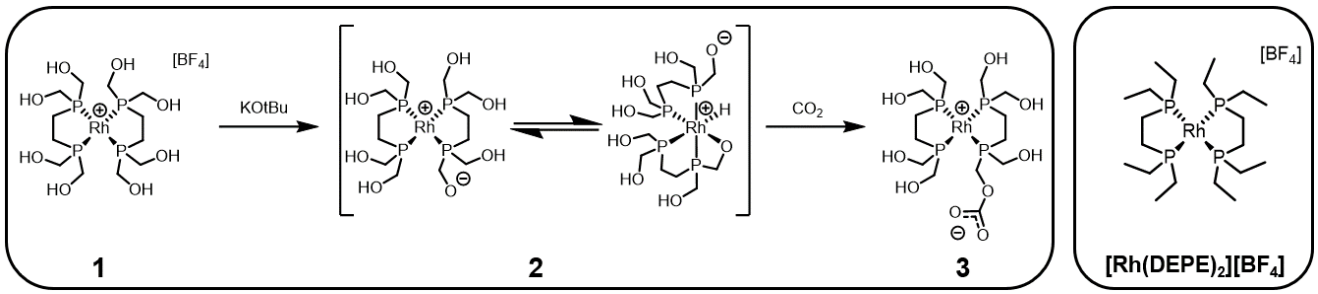

The Rh(I) complex $[Rh(DHMPE)_2][BF_4]$, **1** (Scheme 1), was prepared in 67% yield by combining two equivalents of DHMPE[17] with one equivalent of $[Rh(COD)_2][BF_4]$ in a tetrahydrofuran (THF): dimethylsulfoxide (DMSO) mixture (80:20 v/v). **1** is a square planar Rh(I) complex, as indicated by the presence of a single doublet in the $^{31}P\{^1H\}$ NMR spectrum (δ 62.5 ppm), with a $^1J_{Rh\text{-}P}$ = 121 Hz. (Figure S2). The observed symmetry and Rh-P splitting are consistent with other previously reported square planar Rh(I) bis-phosphine complexes.[18]

Due to their similar electronic and steric properties, $[Rh(DEPE)_2][BF_4]$ was selected for comparison with **1** to elucidate how the proton-responsive nature of DHMPE affects reactivity. DHMPE has similar electron donating ability and steric bulk as 1,2-bis(diethylphosphino)ethane (DEPE). Ni(II) DEPE and DHMPE complexes exhibit near identical reduction potentials and thermodynamic hydricities.[19,20] Likewise, **1** shows similar electronic characteristics to $[Rh(DEPE)_2][BF_4]$, with near identical charge transfer and d–d absorption bands showing very similar energies and molar absorptivities in DMSO (Figure S5).

Under N_2 atmosphere in DMSO, **1** displays two irreversible, one electron reductions at E^{PC}= -2.31 and -2.85 V vs. $[Fe(C_5H_5)_2]^{+/0}$ (black trace, Figure 1). The reduction events display diffusion controlled current (Figure S6) at all measured scan rates, and remain irreversible at scan rates exceeding 1 V/s. This behavior deviates from other Rh(I) bisphosphine complexes, which typically undergo reversible two electron reduction events[21,22] ($[Rh(DEPE)_2][BF_4]$ CVs shown in Figure S8). When KOtBu is added to the solution, the peak current of the first reduction event decreases with increasing base concentration, while the second reduction is affected to a much lesser extent (Figure S9). This behavior suggests that proton transfer is involved in the first reduction step, consistent with the formation of a rhodium hydride species through an EC mechanism.[23,24]

Cyclic voltammograms of **1** under CO_2 atmosphere display an increase in current at the first reduction event (Figure 1). The current passed at the first reduction is roughly doubled and remains consistent across a range of CO_2 concentrations, ranging from atmospheric levels (0.04%) to 100% (Figure 1). This behavior suggests strong CO_2 binding upon reduction of **1**. Without reduction, **1** shows no signs of interaction with CO_2, even under a pure CO_2 atmosphere. By comparison, CVs of $[Rh(DEPE)_2][BF_4]$ show a catalytic current increase in the presence of CO_2 that is highly dependent on CO_2 concentration (Figure S10). While $[Rh(DEPE)_2][BF_4]$ is only capable of CO_2 binding at the Rh center, CO_2 binding with **1** may occur either at the metal center or at an alkoxide (to form an alkyl carbonate species[4,25]), generated via deprotonation of one of the DHMPE arms by the Rh center upon reduction (*vide supra*); these differing modes of CO_2 binding between **1** and $[Rh(DEPE)_2][BF_4]$ may explain their disparate CV behavior.

Complex **1** readily reacts with strong bases in DMSO. Upon addition of one equivalent of potassium *tert*-butoxide (KOtBu), significant spectroscopic changes are observed, and a new species (**2**) is formed (Scheme 1). In the $^{31}P\{^1H\}$ NMR spectrum, the lone doublet observed for **1** splits into 3 distinct doublets at δ = 71.5, 63.2, and 58.9 ppm, with corresponding $^1J_{Rh\text{-}P}$ values of 87, 101, and 71 Hz, respectively (Figure S12). The loss of symmetry and decreased $^1J_{Rh\text{-}P}$ values observed in the $^{31}P\{^1H\}$ spectrum indicate changes to both the coordination geometry and oxidation state of Rh, from square planar Rh(I) to octahedral Rh(III).[18] In addition to the changes observed in the $^{31}P\{^1H\}$ spectrum, the ^1H NMR spectrum shows significant broadening of all resonances, and concomitant growth of a hydride species at -10.62 ppm ($^2J_{P\text{-}H}$ = 130 Hz) that integrates to ~0.3 (Figure S11). Additionally, FTIR spectroscopy of **2** in DMSO shows a stretch at 1944 cm^{-1}, consistent with other reported Rh(III) hydrides (Figure S14).[26]

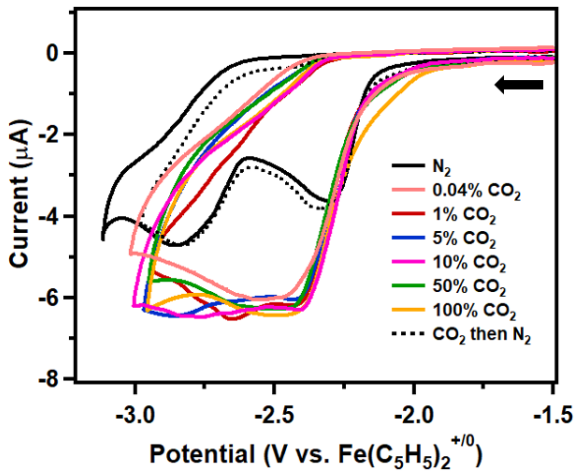

Figure 1. Cyclic voltammograms of **1** under N_2 (black traces) or CO_2 atmospheres of varying concentration, ranging between 0-100% (v/v). Cyclic voltammograms under N_2 atmosphere (i.e. 0% CO_2) were collected before (solid black) or after (dotted black) exposure to CO_2, followed by sparging the solution with N_2. Each voltammogram was recorded using DMSO solutions containing 2mM analyte and 200mM $TBAPF_6$ electrolyte concentrations scanning cathodically (indicated by the black arrow) at a 10 mV/s scan rate.

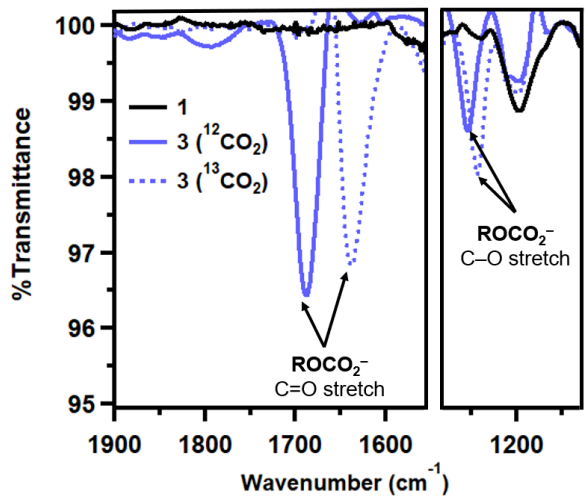

Figure 2. Solution FTIR spectra of **1** (solid black) and **3** in DMSO, generated with $^{12}CO_2$ (solid blue) or $^{13}CO_2$ (dotted blue), showing the frequency ranges corresponding to C=O and C–O stretching.

While unexpected, generation of a Rh(III) hydride species upon ligand deprotonation may be a result of intramolecular oxidative addition of the Rh(I) center into one of the ligand O–H bonds. Changes to the integration of the OH resonance (dropping from 8 to ~6 upon addition of KOtBu to **1**, Figures S1 vs S11) suggest the hydride proton originates from one of the proximal hydroxyl groups. ^{31}P EXSY of **2** shows that the resonances at 71.5 and 58.9 ppm are in exchange with the resonance at 63.2 ppm (Figure S15), which indicates that a rapid equilibrium exists between the two species. The ^{31}P EXSY results, combined with the significant peak broadening and low integration (<1) of the hydride in the ^{1}H NMR, suggest that the oxidative addition reaction (to form the Rh(III) hydride species) is in equilibrium and is close to isoenergetic (Scheme 1). This equilibrium speciation shifts toward the hydride at lower temperatures as shown by ^{1}H VT-NMR of **2** (Figures S16-S18), which is consistent with intramolecular oxidative addition being entropically disfavored. Intermolecular oxidative addition to form a dimeric species can be excluded for the structure of **2** based on the similar diffusional cross section of **1** and **2** as determined by ^{1}H DOSY NMR spectroscopy (Figures S29-S31). **2** is metastable in solution, however, decomposing into unidentified products over several hours at room temperature, or rapidly when exposed to elevated temperatures (>313 K), concomitant with the disappearance of the ^{1}H hydride and ^{31}P resonances, and growth of formate resonances from ligand decomposition (see Figure S19 and page S34 of the SI for further discussion).

Deprotonated complex **2**, on the other hand, is a potent CO_2 capture agent, capable of capture from concentrations below atmospheric levels (≤ 400 ppm). Exposure of **2** to CO_2 mixtures ranging between 0.04 to 100% concentration (v/v) results in complete conversion to a new species, **3** (Scheme 1, Figure S24). **3** shows a single, broad doublet (δ = 61.7 ppm) in the ^{31}P{^{1}H} spectrum, with $^1J_{Rh\text{-}P}$ = 117 Hz (Figure S22). The increase in symmetry and Rh-P coupling suggests that **3** is a square planar Rh(I) species, akin to **1**. Beyond the changes observed with ^{31}P{^{1}H} NMR, the ^{1}H NMR spectrum of **3** shows a significant up field shift of the OH resonances relative to **2**, and associated loss of the hydride resonance at -10.62 ppm (Figures S20 and S21). No further generation of formate was detected by ^{1}H NMR spectroscopy in the conversion of **2** to **3** upon introduction of CO_2, indicating that hydride transfer from **2** to CO_2 does not occur. This is consistent with the previous reports that $[Rh(DEPE)_2H]^{2+}$ and $[Rh(DEPE)_2H_2]^+$ are not sufficiently hydridic to reduce CO_2 to formate.[18] We hypothesize that CO_2 binds to the alkoxide ligand of **2**, which results in a reversal of the OH oxidative addition to form an alkyl carbonate species (**3**) (Scheme 1). The FTIR spectrum of **3** in DMSO features a peak at 1688 cm^{-1}, which is consistent with an alkyl carbonate C=O stretch (Figures 2 and S25).[27,28] When $^{13}CO_2$ is used to generate **3**, the C=O stretch shifts from 1688 to 1637 cm^{-1} (Figures 2, S27, and S28). Furthermore, the ^{13}C{^{1}H} NMR spectrum of **3** generated using $^{13}CO_2$ features a broad resonance at 155 ppm, providing further evidence of alkyl carbonate formation (Figure S26).[25,27,28] Like **1** and **2**, **3** exists as a monomeric species in solution, as evidenced by ^{1}H DOSY experiments (Figures S29-31). Unlike **2** however, **3** is stable in solution for days to weeks at room temperature, and does not show significant signs of decomposition (i.e. further generation of formate and loss of ^{31}P resonances), even at elevated temperatures (Figures S32-S34).

Table 1. Conditions and kinetic parameters for Rh-catalyzed $^{12}C/^{13}C$ isotope exchange reactions.[a]

Precatalyst	Cation	Base	k_{obs}[b] (min^{-1})	$\tau_{1/2}$ (hrs)
$[Rh(DEPE)_2][BF_4]$	Na	N/A	5.1×10^{-4}	18
$[Rh(DEPE)_2][BF_4]$	Na	MO*t*Bu	9.8×10^{-4}	12
1	Li	N/A	9.6×10^{-4}	12
1	Li	MO*t*Bu	4.8×10^{-4}	24
1	Na	N/A	4.6×10^{-4}	25
1	Na	MO*t*Bu	38×10^{-4}	3.0
1	K	N/A	6.8×10^{-4}	17
1	K	MO*t*Bu	51×10^{-4}	2.3
1	K(crypt)	N/A	6.3×10^{-4}	18
1	K(crypt)	MO*t*Bu	7.0×10^{-4}	17

[a] Each catalytic run was performed at 298 K in 0.5 mL DMSO-D_6 containing 1.0 mM [Rh] and ~15 mM $MHCO_2$ under 1.0 Atm. $^{13}CO_2$. Reactions performed in the presence of base contained 1.0 mM [MO*t*Bu]. [b]Measured for $[H^{13}CO_2]^-$ production. See SI for experimental setup and calculations of TOF_i, k_{obs}, and $\tau_{1/2}$.

While the reactivity of the DHMPE Rh(I) hydride with CO_2 could not be probed due to incompatibility with the polar solvents required for its solvation, insights into its reactivity could be obtained through the degenerate catalytic isotope exchange of $[H^{12}CO_2]^-$ and $^{13}CO_2$. Catalytic $^{12}C/^{13}C$ exchange between $[H^{12}CO_2]^-$ and $^{13}CO_2$ serves as an excellent proxy reaction to investigate how secondary sphere effects, associated with deprotonation and CO_2 binding, impact CO_2/formate interconversion. The reaction serves as an good proxy, as it proceeds via the microscopic reverse of CO_2 reduction to generate the metal hydride as an unobserved high energy intermediate, followed by reduction of the isotopically labeled CO_2 through the same transition state (Figure 3A).

When $^{13}CO_2$ is added to a solution of sodium formate and **1** (6.6 mol% relative to formate), ^{13}C incorporation into the formate species is observed via ^{1}H NMR spectroscopy, as the singlet at 8.45 ppm (corresponding to $H^{12}CO_2^-$) decreases in intensity, with concomitant growth of a doublet ($J_{C\text{-}H}$ = 180 Hz) centered at the same chemical shift, consistent with formation of $[H^{13}CO_2]^-$ (Figure 3C). The decrease in ^{12}C formate and corresponding increase in ^{13}C

formate follows a first order approach to equilibrium and can be linearized by plotting the natural logarithm of the difference between ^{13}C formate concentration and ^{13}C formate concentration at equilibrium versus time (Figures S35-S45).

The overall formate concentration remains constant over the course of the experiment, which implies $[H^{13}CO_2]^-$ is generated via $^{12}C/^{13}C$ isotope exchange between $[H^{12}CO_2]^-$ and $^{13}CO_2$ (Figure 3D). The effect of deprotonation and CO_2 binding to the DHMPE ligand on the rate of isotope exchange was then evaluated (Table 1). When no base is present, both **1** and $[Rh(DEPE)_2][BF_4]$ display comparable rates. However, in the presence of one equivalent of base (converting **1** to **3** in situ) a ~10-fold increase in rate is observed. Under the same conditions, $[Rh(DEPE)_2][BF_4]$ only shows a modest (< 2-fold) rate increase (Figure 3D).

As the Rh-H intermediates for both **1** and $[Rh(DEPE)_2][BF_4]$ are anticipated to be significantly more hydridic (and therefore poorer hydride acceptors) than formate (which acts as the hydride donor), generation of the hydride intermediate (denoted as $L_nM–H$ in Figure 3A), along with subsequent hydride delivery to CO_2 on the opposite site of the symmetrical reaction energy profile, is expected to be the rate determining transition state. Indeed, no hydride intermediates are detectable with either catalyst in the presence or absence of base. With this information in mind, three plausible hypotheses can be made to rationalize how the introduction of base increases the rate of degenerate $^{12}C/^{13}C$ exchange catalyzed by **1** (general reaction coordinate diagrams and further discussion for each can be found on pages S34-S38 and Figures S46-48 of the SI). First, the generation of **3** in solution may result in pre-organization of formate/ CO_2 in the transition state via intramolecular hydrogen-bonding networks, or association to a Lewis acidic metal cation (Figure S46). Alternatively, the Rh(I) hydride intermediate of **3** may be more stable than that of **1**, due to structural distortion upon CO_2 binding or chelation of a metal cation (Figure S47). Lastly, **3** may favor an alternative pathway involving low energy Rh(III) mono- and di-hydride species, generated upon intramolecular O-H oxidative addition that is not accessible with **1** (Figure S48).

To better understand the mechanism of the observed rate acceleration, the effect of formate and *tert*-butoxide counter cations was explored. Replacing Na^+ with K^+ ions resulted in a similar order-of-magnitude increase in the rate, however, the homologous Li^+ reaction resulted in a *decrease* in rate upon deprotonation of **1**. This observation is consistent with the hypothesis that the deprotonated Rh complex chelates the counterion in the secondary coordination sphere, and an open coordination site on the larger Na^+ and K^+ ions coordinates formate to pre-organize the transition state for hydride delivery, and by extension, binds CO_2 to accept the hydride in the microscopic reverse reaction (Figure 3B), while the smaller Li^+ ion might be coordinatively saturated by the pendant hydroxyls and carbonate, blocking the secondary sphere Lewis acid effect. To further support the role of coordination to the counterion as integral to the observed rate acceleration, [2.2.2]cryptand was added to the K^+ reaction mixture to encapsulate the ion, which completely negated the accelerating effect of the potassium ion (Table 1, Figure 3E). These counterion effects appear to be inconsistent with the mechanistic hypothesis associated with preferential stabilization of the high energy hydride intermediate, for which little counterion trend would be expected, potentially favoring Li^+ due to increased Lewis acidity. These data do not rule out a similar secondary sphere effect lowering the barrier of a mechanism proceeding via OH oxidative addition and formation of a Rh(III) dihydride intermediate, however, this mechanism is disfavored due to the low hydricity of the Rh(III) dihydride, which is potentially inconsistent with the nature of the high energy intermediate. Further mechanistic evaluation can be found in the SI (pages S37-S38).

$[Rh(DHMPE)_2][BF_4]$, which features proton-responsive DHMPE ligands, shows particular promise for "reactive-capture" CCC approaches. Upon deprotonation, the DHMPE ligand readily binds CO_2 at concentrations as low as 400 ppm. Although solvent

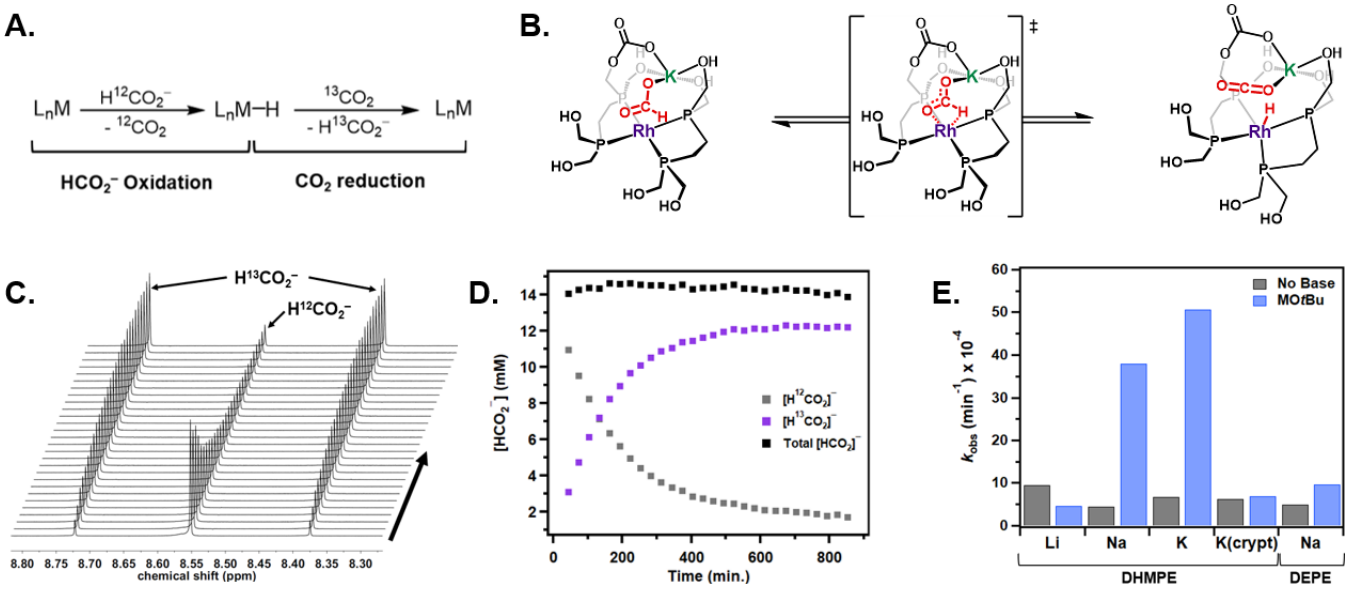

Figure 3. A.) generic reaction scheme for transition-metal catalyzed $^{12}C/^{13}C$ isotope exchange between $[H^{12}CO_2]^-$ and $^{13}CO_2$. B.) proposed mechanism for Rh–H formation where chelation of a potassium ion with **3** facilitates pre-organization of formate/CO_2 with the Rh metal center. C.) ^1H NMR kinetic trace and D.) $[HCO_2]^-$ vs. time graph for $^{12}C/^{13}C$ isotope exchange between $KH^{12}CO_2$ and $^{13}CO_2$. catalyzed by **1** in the presence of 1 eq. KO*t*Bu. E.) comparison of measured k_{obs} values for $[H^{13}CO_2]^-$ generation using $[Rh(L)_2][BF_4]$ catalysts (where L= DEPE or DHMPE) using various $M[H^{12}CO_2]$ salts (where M = Li, Na, K, or K(crypt)) in the presence or absence of the corresponding base (MO*t*Bu).

limitations prevented direct investigation into CO_2 reduction reactions, indirect investigation via catalytic $^{12}C/^{13}C$ exchange shows significant rate enhancements when the DHMPE ligand is deprotonated to bind CO_2 and lowering the barrier to hydride transfer. The cation-dependent activity of **1** in the presence of base suggests CO_2 binding allows pre-organization of formate/CO_2 in the transition state. These findings provide valuable insight to enhance the kinetics of CO_2 reduction with catalysts unamenable to previously reported approaches (i.e. non-metal clusters that do not go through "outer-sphere" or concerted hydride transfer pathways).

ASSOCIATED CONTENT

Supporting Information.

The Supporting Information is available free of charge at URL

General methods; detailed experimental procedures; extended discussion of key analysis and proposed mechanisms; and supplemental figures (PDF).

AUTHOR INFORMATION

Corresponding Author

David M. Kaphan — Chemical Sciences and Engineering Division, Argonne National Laboratory, Lemont, Illinois 60439, United States; orcid.org/0000-0001-5293-7784; Email: kaphand@anl.gov

Authors

Jeffrey M. Barlow — *Chemical Sciences and Engineering Division, Argonne National Laboratory, Lemont, Illinois 60439, United States;* orcid.org/0000-0002-9536-8021.

Nikita Gupta — *Department of Chemistry, University of Illinois Chicago, Chicago, Illinois 60607, United States; Chemical Sciences and Engineering Division, Argonne National Laboratory, Lemont, Illinois 60439, United States.*

Ksenija D. Glusac — *Department of Chemistry, University of Illinois Chicago, Chicago, Illinois 60607, United States; Chemical Sciences and Engineering Division, Argonne National Laboratory, Lemont, Illinois 60439, United States;* orcid.org/0000-0002-2734-057X.

David M. Tiede — *Chemical Sciences and Engineering Division, Argonne National Laboratory, Lemont, Illinois 60439, United States;* orcid.org/0000-0002-2784-4954.

Funding Sources

This work is supported by the U.S. Department of Energy (DOE), Office of Science, Office of Basic Energy Science, Division of Chemical Sciences, Geosciences, and Biosciences, through Argonne National Laboratory under Contract No. DE-AC02-06CH11357.

ACKNOWLEDGMENT

We would like to thank Dr. John V. Muntean for assistance with NMR, particularly ^{31}P EXSY experiments. We would also like to thank Dr. Karen L. Mulfort and Dr. Zhulin (Sam) Xie for insightful discussions.

REFERENCES

(1) Agency, I. E. *World Energy Outlook 2019*; 2019.

(2) Sullivan, I.; Goryachev, A.; Digdaya, I. A.; Li, X.; Atwater, H. A.; Vermaas, D. A.; Xiang, C. Coupling Electrochemical CO_2 Conversion with CO_2 Capture. *Nat. Catal.* **2021**, *4* (11), 952–958.

(3) Yamazaki, Y.; Miyaji, M.; Ishitani, O. Utilization of Low-Concentration CO_2 with Molecular Catalysts Assisted by CO_2-Capturing Ability of Catalysts, Additives, or Reaction Media. *J. Am. Chem. Soc.* **2022**, *144* (15), 6640–6660.

(4) Heldebrant, D. J.; Koech, P. K.; Glezakou, V.-A.; Rousseau, R.; Malhotra, D.; Cantu, D. C. Water-Lean Solvents for Post-Combustion CO_2 Capture: Fundamentals, Uncertainties, Opportunities, and Outlook. *Chem. Rev.* **2017**, *117* (14), 9594–9624.

(5) Sanz-Pérez, E. S.; Murdock, C. R.; Didas, S. A.; Jones, C. W. Direct Capture of CO_2 from Ambient Air. *Chem. Rev.* **2016**, *116* (19), 11840–11876.

(6) Forse, A. C.; Milner, P. J. New Chemistry for Enhanced Carbon Capture: Beyond Ammonium Carbamates. *Chem. Sci.* **2021**, *12* (2), 508–516.

(7) Wang, C.; Luo, H.; Jiang, D.; Li, H.; Dai, S. Carbon Dioxide Capture by Superbase-Derived Protic Ionic Liquids. *Angew. Chemie Int. Ed.* **2010**, *49* (34), 5978–5981.

(8) Siegel, R. E.; Pattanayak, S.; Berben, L. A. Reactive Capture of CO_2: Opportunities and Challenges. *ACS Catal.* **2023**, *13* (1), 766–784.

(9) Liu, Q.; Wu, L.; Gülak, S.; Rockstroh, N.; Jackstell, R.; Beller, M. Towards a Sustainable Synthesis of Formate Salts: Combined Catalytic Methanol Dehydrogenation and Bicarbonate Hydrogenation. *Angew. Chemie Int. Ed.* **2014**, *53* (27), 7085–7088.

(10) Li, Y.; Ding, K. 1.8 Catalytic Reduction of Carbonates. *Catalytic Reduction in Organic Synthesis 1*. 1st edition. Georg Thieme Verlag KG: Stuttgart 2018.

(11) Zheng, X.; Drummer, M. C.; He, H.; Rayder, T. M.; Niklas, J.; Weingartz, N. P.; Bolotin, I. L.; Singh, V.; Kramar, B. V; Chen, L. X.; Hupp, J. T.; Poluektov, O. G.; Farha, O. K.; Zapol, P.; Glusac, K. D. Photoreactive Carbon Dioxide Capture by a Zirconium–Nanographene Metal–Organic Framework. *J. Phys. Chem. Lett.* **2023**, *14* (18), 4334–4341.

(12) Weerasooriya, R. B.; Gesiorski, J. L.; Alherz, A.; Ilic, S.; Hargenrader, G. N.; Musgrave, C. B.; Glusac, K. D. Kinetics of Hydride Transfer from Catalytic Metal-Free Hydride Donors to CO_2. *J. Phys. Chem. Lett.* **2021**, *12* (9), 2306–2311.

(13) Heimann, J. E.; Bernskoetter, W. H.; Hazari, N.; Mayer, J. M. Acceleration of CO_2 Insertion into Metal Hydrides: Ligand, Lewis Acid, and Solvent Effects on Reaction Kinetics. *Chem. Sci.* **2018**, *9* (32), 6629–6638.

(14) Heimann, J. E.; Bernskoetter, W. H.; Hazari, N. Understanding the Individual and Combined Effects of Solvent and Lewis Acid on CO_2 Insertion into a Metal Hydride. *J. Am. Chem. Soc.* **2019**, *141* (26), 10520–10529.

(15) Hazari, N.; Heimann, J. E. Carbon Dioxide Insertion into Group 9 and 10 Metal–Element σ Bonds. *Inorg. Chem.* **2017**, *56* (22), 13655–13678.

(16) Pattanayak, S.; Berben, L. A. Pre-Equilibrium Reaction Mechanism as a Strategy to Enhance Rate and Lower Overpotential in Electrocatalysis. *J. Am. Chem. Soc.* **2023**, *145* (6), 3419–3426.

(17) Nieckarz, G. F.; Weakley, T. J. R.; Miller, W. K.; Miller, B. E.; Lyon, D. K.; Tyler, D. R. Generation of 19-Electron Adducts in Aqueous Solution Using the Water-Soluble $(HOCH_2)_2PCH_2CH_2P(CH_2OH)_2$ Ligand. *Inorg. Chem.* **1996**, *35* (6), 1721–1724.

(18) Wilson, A. D.; Miller, A. J. M.; DuBois, D. L.; Labinger, J. A.; Bercaw, J. E. Thermodynamic Studies of $[H_2Rh(Diphosphine)_2]^+$ and $[HRh(Diphosphine)_2(CH_3CN)]^{2+}$ Complexes in Acetonitrile. *Inorg. Chem.* **2010**, *49* (8), 3918–3926.

(19) Curtis, C. J.; Miedaner, A.; Ellis, W. W.; DuBois, D. L. Measurement of the Hydride Donor Abilities of $[HM(Diphosphine)_2]^+$ Complexes (M = Ni, Pt) by Heterolytic Activation of Hydrogen. *J. Am. Chem. Soc.* **2002**, *124* (9), 1918–1925.

(20) Tsay, C.; Livesay, B. N.; Ruelas, S.; Yang, J. Y. Solvation Effects on Transition Metal Hydricity. *J. Am. Chem. Soc.* **2015**, *137* (44), 14114–14121.

(21) Price, A. J.; Ciancanelli, R.; Noll, B. C.; Curtis, C. J.; DuBois, D. L.; DuBois, M. R. $HRh(Dppb)_2$, a Powerful Hydride Donor. *Organometallics* **2002**, *21* (22), 4833–4839.

(22) Lilio, A. M.; Reineke, M. H.; Moore, C. E.; Rheingold, A. L.; Takase, M. K.; Kubiak, C. P. Incorporation of Pendant Bases into $Rh(Diphosphine)_2$ Complexes: Synthesis, Thermodynamic Studies, And Catalytic CO_2 Hydrogenation Activity of $[Rh(P_2N_2)_2]^+$ Complexes. *J. Am. Chem. Soc.* **2015**, *137* (25), 8251–8260.

(23) Zanello, P. *Inorganic Electrochemistry: Theory, Practice and Application*; The Royal Society of Chemistry: Cambridge, UK, 2003.

(24) Bard, A. J.; Faulkner, L. R. *Electrochemical Methods: Fundamentals and Application*, 2nd ed.; Swain, E., Ed.; John Wiley & Sons, Inc.:

Hoboken, NJ, 2001.
(25) Phan, L.; Chiu, D.; Heldebrant, D. J.; Huttenhower, H.; John, E.; Li, X.; Pollet, P.; Wang, R.; Eckert, C. A.; Liotta, C. L.; Jessop, P. G. Switchable Solvents Consisting of Amidine/Alcohol or Guanidine/Alcohol Mixtures. *Ind. Eng. Chem. Res.* **2008**, *47* (3), 539–545.
(26) Morris, R. H. Estimating the Wavenumber of Terminal Metal-Hydride Stretching Vibrations of Octahedral D^6 Transition Metal Complexes. *Inorg. Chem.* **2018**, *57* (21), 13809–13821.
(27) Barlow, J. M.; Yang, J. Y. Oxygen-Stable Electrochemical CO_2 Capture and Concentration with Quinones Using Alcohol Additives. *J. Am. Chem. Soc.* **2022**, *144* (31), 14161–14169.
(28) Mizen, M. B.; Wrighton, M. S. Reductive Addition of CO_2 to 9,10-Phenanthrenequinone. *J. Electrochem. Soc.* **1989**, *136* (4), 941–946.

Insert Table of Contents artwork here